New Phytologist

Research

Relieving the transfusion tissue traffic jam: a network model of radial transport in conifer needles

Melissa H. Mai[1], Chen Gao[2], Peter A. R. Bork[3], N. Michele Holbrook[1], Alexander Schulz[2] and Tomas Bohr[3]

[1]Department of Organismic and Evolutionary Biology, Harvard University, Cambridge, MA 02138, USA; [2]Department of Plant and Environmental Sciences, University of Copenhagen, 1871, Frederiksberg C, Denmark; [3]Department of Physics, Technical University of Denmark, 2800, Kongens Lyngby, Denmark

Authors for correspondence:
Melissa H. Mai
Email: melissamai@g.harvard.edu

Tomas Bohr
Email: tbohr@fysik.dtu.dk

Received: *15 July 2024*
Accepted: *24 September 2024*

New Phytologist (2024)
doi: 10.1111/nph.20189

Key words: conifers, gymnosperms, modeling, phloem loading, solute transport, transfusion tissue.

Summary

- Characteristic of all conifer needles, the transfusion tissue mediates the radial transport of water and sugar between the endodermis and axial vasculature. Physical constraints imposed by the needle's linear geometry introduce two potential extravascular bottlenecks where the opposition of sugar and water flows may frustrate sugar export: one at the vascular access point and the other at the endodermis.
- We developed a network model of the transfusion tissue to explore how its structure and composition affect the delivery of sugars to the axial phloem. To describe extravascular transport with cellular resolution, we construct networks from images of *Pinus pinea* needles obtained through tomographic microscopy, as well as fluorescence and electron microscopy.
- The transfusion tissue provides physically distinct pathways for sugar and water, reducing resistance between the vasculature and endodermis and mitigating flow constriction at the vascular flank. Dissipation of flow velocities through the transfusion tissue's branched structure allows for bidirectional transport of an inbound diffusive sugar flux against an outbound advective water flux across the endodermis.
- Our results clarify the structure–function relationships of the transfusion tissue under conditions free of physiological stress. The presented model framework is also applicable to different transfusion tissue morphologies in other gymnosperms.

Introduction

Plants synthesize sugars via photosynthesis, using carbon dioxide absorbed from the atmosphere. In conifers, the loading of sugars into the phloem is thought to be an entirely passive process, driven by the concentration gradient of sugar between the photosynthetic mesophyll and the phloem (Liesche & Schulz, 2012; Liesche, 2017). Due to the conifer needle's long, narrow geometry, uniform axial loading of the phloem along a single central vein will cause stagnation beyond an effective distance of a few centimeters upstream of the needle base (Zwieniecki *et al.*, 2006; Rademaker *et al.*, 2017, 2021). To prevent this stagnation, needles adopt a tiered architecture in their axial venation (Liesche *et al.*, 2021) (Fig. 1a). Moving down the needle from tip to base, new conduits are observed at the periphery of the vascular bundle at regular intervals, consistent with observations of elongation from a meristem at the needle base (Ghouse *et al.*, 1972; Sands & Correll, 1976; Guzicka *et al.*, 2023). This infrastructure longitudinally segments the needle into discrete loading zones that, individually, are short enough to prevent stagnation (Liesche *et al.*, 2021). However, this solution to the axial transport problem introduces a new challenge in extravascular, radial transport. Photosynthesis occurs along most of the needle's circumference, yet loading only occurs on the outer edge, or flank, of the vascular bundle (Fig. 1a(iii); arrows, Fig. 2). As a result, sugar has only two points of entry into the phloem (Heimerdinger, 1951; Gao *et al.*, 2023). This introduces a bottleneck within the radial transport pathway near the center of the needle. At the same time, water must flow in the opposite direction from the xylem to irrigate the mesophyll and replace water lost to transpiration. Tracer experiments show that water also flows through focused points at the flanks of the xylem before spreading out to irrigate the entire perimeter (unpublished).

Toward the exterior of the needle, transport faces another bottleneck (Fig. 1b). The endodermis, forming the bundle sheath, serves as the gatekeeper between the vasculature and the photosynthetic mesophyll. Water moves through the endodermis into the mesophyll to support photosynthesis and transpiration, while sugar moves in the opposite direction for export. In *Pinus* needles, the endodermis is sealed by a Casparian strip, which blocks apoplastic (extracellular) flow (Haberlandt, 1914; Gao *et al.*, 2023). By preventing flow through the cell wall, the Casparian strip forces both water and sugar to travel simultaneously through the lumen of the endodermis, despite moving in opposite directions.

Here we explore how the radial infrastructure of the needle reconciles the two traffic jams of these flows: one at the axial

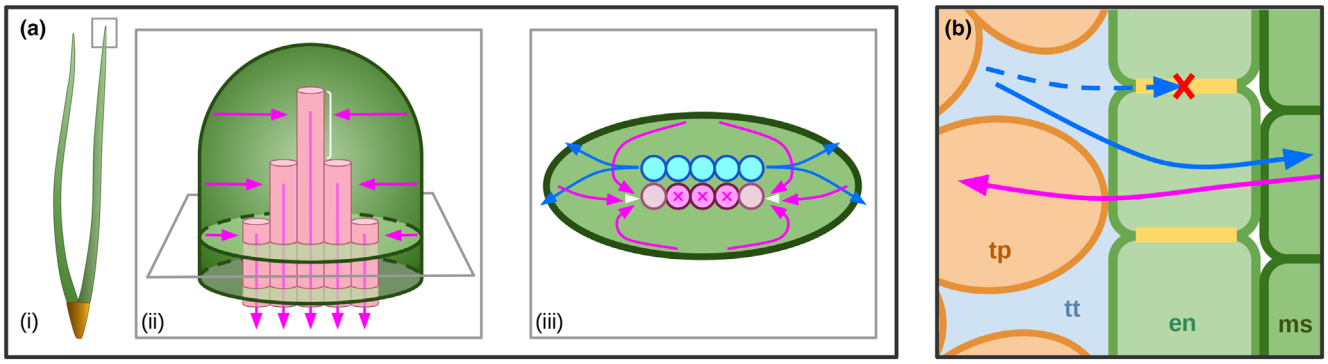

Fig. 1 Schematics of the two bottlenecks in the extravascular transport of sugar (magenta) and water (blue) in a conifer needle. (a) To avoid stagnation of axial sugar transport in a long, narrow needle (i), vascular tiers provide dedicated loading zones (white bracket) for each longitudinal segment, with new vascular conduits appearing at the periphery of the bundle from tip to base and blocking the loading of interior conduits (ii). (iii) However, this introduces a new challenge in the radial (transverse) transport pathway by forcing sugar flows from the entire perimeter to focus into only two phloem loading points at the outermost conduits (white arrows). Meanwhile, water moves in the opposite direction for irrigation and transpiration. (b) A Casparian strip (yellow) at the endodermis blocks apoplastic flow, forcing water and sugar countercurrents to travel simultaneously through the lumen of the endodermal cells (en) between the transfusion parenchyma (tp) or transfusion tracheids (tt) and the mesophyll (ms).

vasculature and the other at the endodermis. Though we explore this from a structural standpoint, we acknowledge that needles may also approach these problems through temporal separation of the transpiration and sugar streams. Diurnal variations in leaf starch content have been studied in both conifers (Webb & Kilpatrick, 1993; Liesche *et al.*, 2021) and angiosperms (Klages *et al.*, 2001; Ribeiro *et al.*, 2012; Tixier *et al.*, 2018; Gersony *et al.*, 2020). Starch synthesis during the day sequesters excess sugars to prevent excessive osmotic buildup (Furze *et al.*, 2018) and end-product inhibition of photosynthesis (Goldschmidt & Huber, 1992). When photosynthesis stops at night, starches can be hydrolyzed back into soluble sugar to be exported from the needle without an opposing transpiration stream. Starch accumulation cannot solve the axial transport problem, as the phloem lacks the relevant enzymes, but tissues outside the vasculature may serve as temporary storage to help evacuate sugars from the mesophyll. While this has been suggested as a solution, we propose that there is a physical, instead of biochemical, solution, motivated by the unique anatomy of conifer needles.

Characteristic of all gymnosperms is not only an unbranched leaf vascular design but also an anatomical feature known as the transfusion tissue, which lies between the axial vasculature and the endodermis (Fig. 2). Fossil evidence suggests that the transfusion tissue evolved by the late Paleozoic (Yang *et al.*, 2022), with precursors appearing in *Cordaites* during the late Carboniferous (Stopes, 1903). Today, the transfusion tissue is ubiquitous among conifers, *Ginkgo*, and cycads, with substantial diversity in its extent and arrangement within the leaf (Jeffrey & Torrey, 1916; Griffith, 1957; Ghouse & Yunus, 1974, 1975; Esau, 1977; Carvalho *et al.*, 2017). The transfusion tissue can adopt one of seven morphological classes, including, for example, the *Pinus*-type that encircles the entire bundle, the *Pseudotsuga*-type that adopts a U-shaped arc around the abaxial side of the bundle, and the wing-like *Cupressus*-type that extends laterally from the flanks of the axial vasculature (Hu & Yao, 1981). Transfusion tissue consists of two cell types: transfusion tracheids and transfusion parenchyma (Fig. 2b,c). Transfusion tracheids are dead, water-conducting cells that are generally regarded as extensions of the xylem. Transfusion parenchyma are living cells that conduct sugar symplasmically to the phloem loading point, where Strasburger cells, historically labeled as *albuminous cells*, aid with loading (Worsdell, 1897).

While the structure of the transfusion tissue has been well described, its physiological function has been sparsely explored, considered primarily for its role as a site for nutrient retrieval (Canny, 1993) or in the context of stress responses. For example, due to their thinner walls relative to those of the xylem, transfusion tracheids have been observed collapsing under drought and recovering upon rehydration as a 'hydraulic circuit breaker' (Brodribb & Holbrook, 2005; Zhang *et al.*, 2014; Bouche *et al.*, 2016). Analogous behavior is found in other plant taxa, such as the reversible collapse of smallest-order veins in angiosperms (Zhang *et al.*, 2016, 2023) or the complete disconnection of the vascular bundle from the photosynthetic tissue of lycopods during drought (Cardoso *et al.*, 2020). Having a tissue serve as a hydraulic shock absorber protects the axial xylem from embolism, especially in evergreen conifer needles that persist over multiple years and experience several freeze–thaw cycles (Chang *et al.*, 2021). Yet, the presence of transfusion tissue in deciduous conifers, or those that live in warmer climates, suggests it provides additional advantages.

Moreover, the role of its distinctive spatial organization in the functioning of the needle has not yet been explained. The transfusion tracheid and transfusion parenchyma systems are often treated as extensions of the xylem and phloem, respectively, and were hypothesized to share their ontogenetic origin with the primary vasculature (Worsdell, 1897). Later studies questioned the origin of the transfusion tissue in the procambium (Carter, 1911; Griffith, 1957; Gifford & Foster, 1996; Aloni *et al.*, 2013). Its confinement by the endodermis, however, emphasizes that it is exclusively responsible for the two-way traffic of water and sugar between the vasculature and photosynthetic tissue (Esau, 1977).

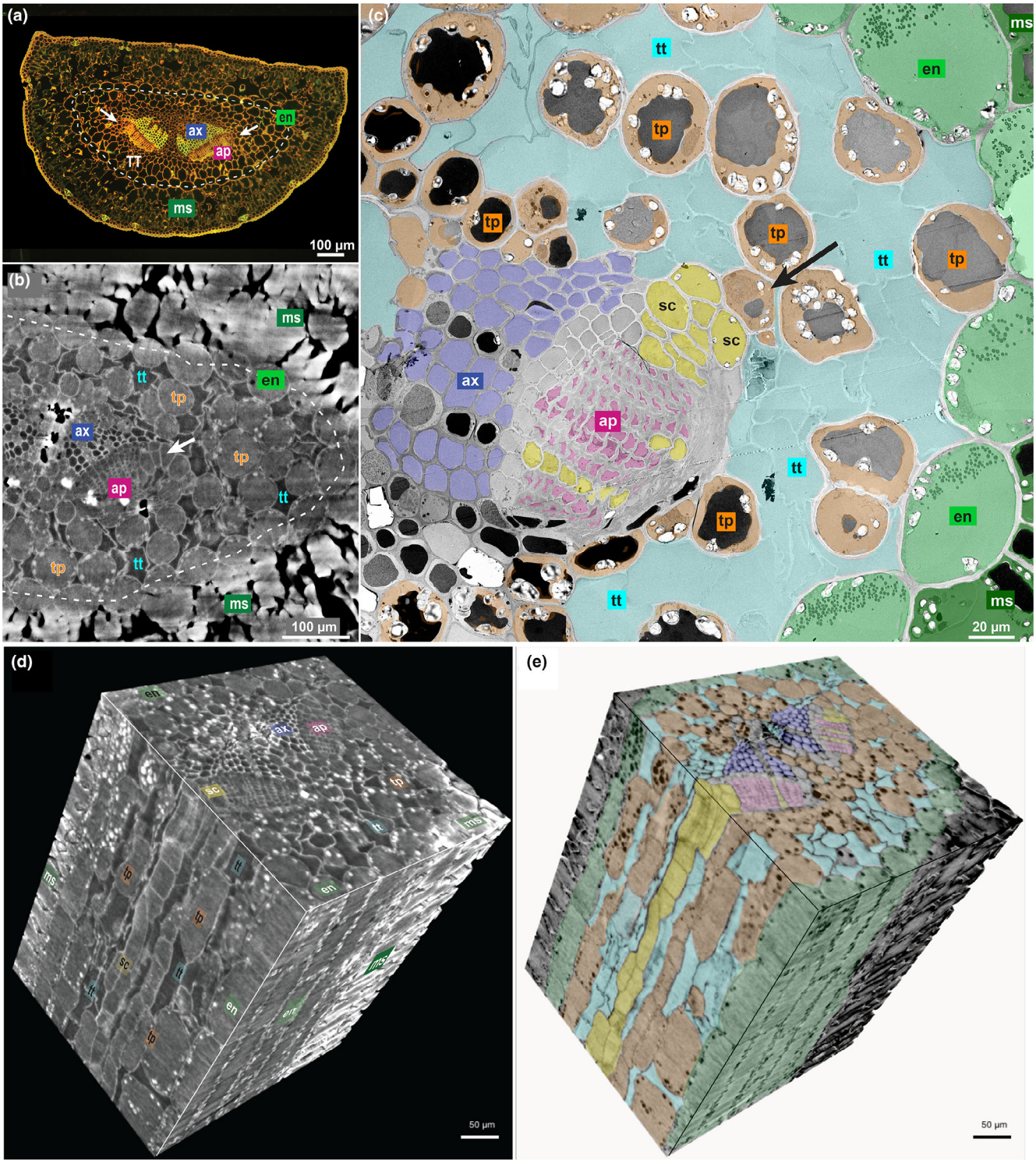

Fig. 2 Three-dimensional architecture of a *Pinus pinea* needle as seen in fixed (a, c) and live (b, d, e) material. Tissue distribution is revealed in cross sections and in 3D: confocal, coriphosphine-stained image (a), µX-ray computed tomograph (b), and transmission electron micrograph (c), and in 3D visualizations with original tomography contrast (d) and tissue painting (e), respectively. Labels and colors identify the tissues and cell types covered by the network model: axial xylem (ax, blue); axial phloem (ap, magenta); transfusion tissue (TT) consisting of transfusion tracheids (tt, cyan) and transfusion parenchyma (tp, orange); endodermis (en, light green); and mesophyll (ms, dark green). Strasburger cells (sc, yellow) are also indicated, though they are not explicitly described in the model. The vascular flanks, where loading and unloading occur, are indicated by the arrows. Starch granules are clearly visible in the transfusion parenchyma and endodermis of (c). Bars: (a, b) 100 µm; (c) 20 µm; (d, e) 50 µm.

A striking distinction between the transfusion tissue and the primary vasculature is that the transfusion tracheid and transfusion parenchyma cells do not form spatially distinct cell files, as the xylem and phloem do. Rather, they are highly interdigitated within each other, sharing a large interfacial surface area between the two cell systems (Huber, 1947; Gao *et al.*, 2023).

We present a network-based mathematical model of the transfusion tissue, built to understand its role in mediating the radial two-way transport of sugar and water within the needle. As this system is difficult to probe experimentally, our computational approach resolves intercellular flows of sugar and water through the transfusion tissue, allowing us to study its hydraulic function even with uncertainty in the parameter space. We simulate networks of varying sizes and compositions to explore the impact of the transfusion tissue on transport in a functional needle. By perturbing intercellular connections within anatomically informed networks of *Pinus*-type needles, we find that the transfusion tissue's structure and heterogeneous composition alleviate the constriction of flow at both the axial vasculature's focused access points and the endodermis by dispersing flow velocities and physically separating the opposing currents of sugar and water.

Materials and Methods

Plant material

For fluorescence and electron microscopy, *Pinus pinea* L. branches were collected from a 4-yr-old tree in the glasshouse of the University of Copenhagen, Denmark, and, for tomographic microscopy, from a tree in the old Botanical Garden of the University of Zürich.

Fluorescence and electron microscopy

After gently removing the epidermis, 10-mm needle segments were immediately immersed into Karnovsky's fixative (4% (w/v) paraformaldehyde and 5% (w/v) glutaraldehyde in 0.1 M sodium cacodylate buffer, pH 7.4), and fixed according to Hunziker & Schulz (2019). To avoid preparation artefacts, 3-mm ends of each segment were discarded. After polymerization, the samples were trimmed for fluorescence and electron microscopy. Semithin transverse sections of 2-µm thickness were transferred onto drops of distilled water placed on a microscope slide, dried on a heating plate and stained with 3% (w/v) Coriphosphine O (CAS 5409-37-0; TCI Europe, Zwijndrecht, Belgium) for 5 min. Images were taken with a wide-field fluorescence microscope (Nikon Eclipse 80i, Amsterdam, the Netherlands) at 450–490 nm excitation and 520 nm long-pass emission filters. Ultrathin sections from *P. pinea* of 70 nm thickness were cut with a diamond knife and ultramicrotome (EM UC7; Leica Microsystems, Wetzlar, Germany). The sections were transferred to film-coated single-slot grids (FCF2010-CU; Electron Microscopy Sciences, Hatfield, PA, USA) and postcontrasted with uranyl-less solution for 3 min and lead citrate solution for 3 min with thorough washing after each step. For transmission electron microscopy (TEM), a Thermo Fisher Talos L120C G2 was used at 120 kV acceleration voltage for an overview, stitched from 9 image tiles with ×510 primary magnification using Map3 software.

Tomographic microscopy at the TOMCAT beamline, Paul Scherrer Institute, Switzerland

Needles were detached from the branch under water and immediately transferred to 2 ml Eppendorf tubes with Milli-Q water. The needles were held upright during rotation in a chamber while immersed in the Eppendorf tube (Gao *et al.*, 2023). For imaging, the middle, tip, and base segment were targeted, with 1000 projections acquired at 21 keV over 180° rotation around the needle center using a ×20 objective, resulting in an effective pixel size of 0.325 µm. Reconstruction of the scans followed the gridrec and paganing algorithms established at the TOMCAT beamline, providing *z*-stacks of 2160 needle cross sections. To avoid optical artefacts at the ends of the scanned area, 2D-segmentations were taken at cross section 500, 1000 and 1500. The dimensions of the scanned image cube were *c.* $0.7 \times 0.7 \times 0.7$ mm. To visualize the 3D structure of the interior of the needle, we imported an 0.5 mm high *z*-stack (1538 cross sections) into the open-source software FluoRender (https://www.sci.utah.edu/software/fluorender.html). Tissue painting was done on a contrast-inverted tomograph using Adobe Photoshop.

Model description

The model explores the potential interference of the sugar and water flows, whose net movements run in opposite directions between the axial vasculature and the photosynthetic mesophyll. While the water flow must spread out from a concentrated source at the flank of the axial xylem to irrigate the needle's perimeter, sugar funnels in from the circumferential region of the photosynthetic mesophyll into a concentrated loading point at the flank of the axial phloem. To avoid needing to specify spatial and geometrical details of the needle, we describe the stele (i.e. the axial vasculature and transfusion tissue), the surrounding endodermis, and photosynthetic mesophyll as a nodal network. Though informed by anatomy, the model does not rely on the exact positions or shapes of cells but rather on a description of each cell's neighbors. This approach is justified by the assumption that cytoplasmic streaming keeps the cytosol well mixed and that the intercellular connections of the plasmodesmata, aquaporins, or bordered pits account for most of the resistance to flow (Goldstein & van de Meent, 2015). Therefore, the actual transport distance becomes less important than the discrete number of cells that are traversed (Rockwell *et al.*, 2018).

Nodal networks were constructed from tomographic micrographs of 12 needles, selecting cross sections from each needle's lower, middle, and upper thirds. Due to the needles' bilateral symmetry, networks were generated from one half of each cross section, retaining only sections where the endodermis was entirely visible, to create a total of 66 total networks. Using MATLAB 2022b's Image Processing Toolbox, cells in each

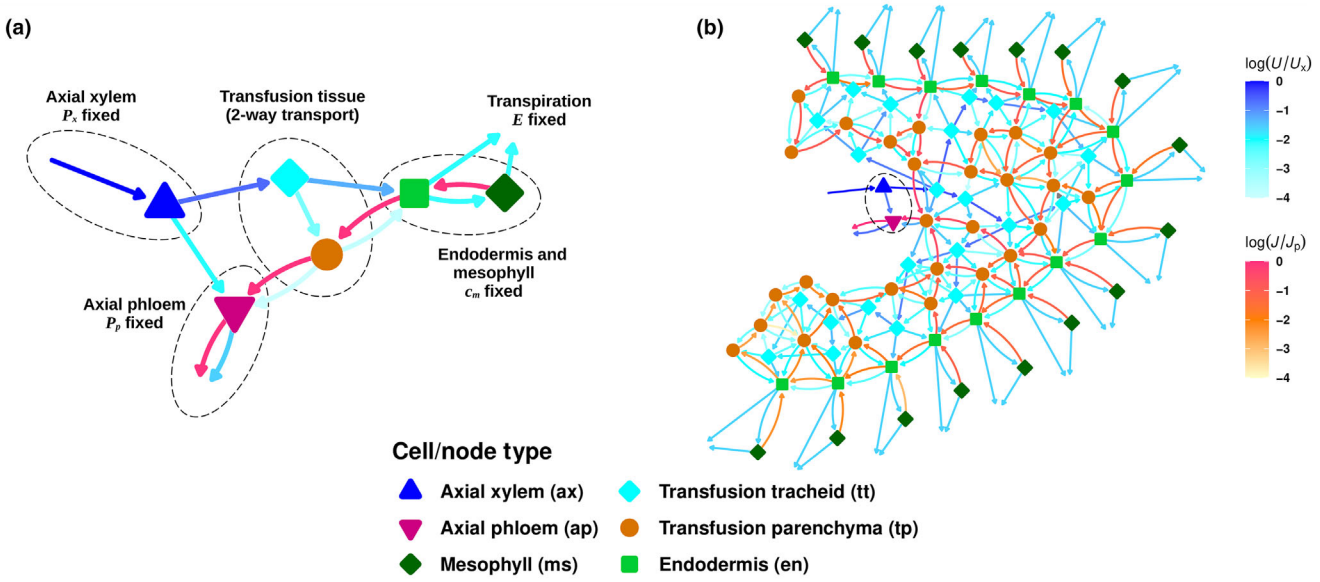

Fig. 3 Diagrams of the steady-state solutions of the transfusion tissue network model. Node shape and color correspond to cell type. The arrows indicate water (U, cyan to blue) and sugar (J, yellow to red) flows between cells, normalized to the flows through the axial xylem (U_x) and axial phloem (J_p), respectively. (a) The fundamental network model, with a summary of boundary conditions. (b) A representative network constructed from a *Pinus pinea* needle, $\xi_{pd} = \xi_{aq} = 0.1$. The axial vasculature (ax, ap) is indicated by the dashed circle. An overlay of this network onto its original micrograph is presented in the Supporting Information.

image were manually identified by type. Connections between adjacent cells were then documented in an adjacency matrix, which, together with a vector of cell identities, formed the primary inputs for the mathematical model.

A diagram of the basic model is presented in Fig. 3(a), and Table 1 provides the relevant parameters. Each node in the network corresponds to a cell, defined by its cell type and described by its pressure and sugar concentration. To allow for the extension of the model to nonsteady conditions, cellular starch content is also included, even though its inclusion does not affect the steady-state solution. The cell types include the dead tracheary elements (axial xylem (ax) and transfusion tracheid (tt)) and the living cells (axial phloem (ap), transfusion parenchyma (tp), endodermis (en), and mesophyll (ms)). The edges, or connections between nodes, correspond to intercellular connections, defined by the identities of the paired cells, and parameterize the water and sugar flows between cells. Water flows through each connection (blue arrows, Fig. 3a), but sugar can only flow between living cells (red arrows, Fig. 3a).

Governing equations

Between two nodes i and j, the water flow U_{ij} is described by the Kedem–Katchalsky equation for flow across a membrane (Kedem & Katchalsky, 1958):

$$U_{ij} = \xi_{ij}\left(\Delta P_{ij} - \sigma_{ij} RT \Delta c_{ij}\right) \qquad \text{Eqn 1}$$

where U_{ij} indicates movement of water from node j into node i, with $U_{ij} = -U_{ji}$. The model equations are dimensionless. Table 1 summarizes the corresponding dimensional values and units for the model's variables and parameters, which are made dimensionless before entering the model (Supporting Information Notes S1). Eqn 1 describes the driving force for water flow as the difference in water potentials, multiplied by a hydraulic conductivity ξ_{ij}. The water potential consists of a pressure (ΔP_{ij}) and osmotic ($-\sigma_{ij} RT \Delta c_{ij}$) component, with R as the ideal gas constant, T the temperature, and σ_{ij} the reflection coefficient (discussed below). While the van't Hoff approximation for the osmotic potential, RTc, is valid only in the limit of dilute solutions, it is used here since we consider concentrations only up to 0.5 M.

The conductivity ξ_{ij} is a symmetric ($\xi_{ij} = \xi_{ji}$) edge property that is defined by the identities of nodes i and j. Between tracheary elements (ax, tt), bordered pits mediate the flow between cells, offering low resistance (high conductivity) for water flow. Between two living cells (ap, tp, en, ms), water moves either through membrane-bound aquaporins or through plasmodesmata, which provide cytoplasmic continuity between cells. Between a living and a tracheary cell, water travels exclusively through aquaporins embedded in the membrane of the living cell and pits of the tracheary cell. Flow through aquaporins and plasmodesmata encounters higher resistance compared to flow through the large bordered pits. Within the model, we normalize all conductivities to the conductivity through the bordered pits, such that $\xi_{bp} = 1$, and explore the parameter space for the conductivities across interfaces mediated by only aquaporins (ξ_{aq}) and by both plasmodesmata and aquaporins (ξ_{pd}). Table 2 summarizes these relationships.

The reflection coefficient σ_{ij} ($0 \leq \sigma_{ij} \leq 1$) is a symmetric quantity that describes the permeability of solutes (i.e. sugar) across an

New Phytologist

Table 1 Model variables and parameters with their corresponding units.

Quantity	Symbol	Value	Units
Concentration	c	–	mol m^{-3}
Effective diffusion	ωRT	–	m^3 s^{-1}
Water potential	ψ	–	Pa
Turgor pressure	P	–	Pa
Water flow	U	–	m^3 s^{-1}
Sugar flux	J	–	mol s^{-1}
Total transpiration	E	–	mol s^{-1}
Starch content	s	–	kg m^{-3}
Relative intercellular hydraulic conductivity	ξ	$0 \le \xi \le 1$	–
Reflection coefficient	σ	$0 \le \sigma \le 1$	–
Mesophyll concentration	c_m	500	mol m^{-3}
Free diffusion of sucrose	D_{free}	2.3×10^{-10}	m^2 s^{-1}
Gas constant	R	8.314	m^3 Pa K^{-1} mol^{-1}
Temperature	T	298.15	K
Molar volume of water	$\bar{v}$	1.807×10^{-5}	m^3 mol^{-1}
Sucrose molar mass	M_s	0.34	kg mol^{-1}
Starch kinetics			
Michaelis constant	K_m	500	mol m^{-3}
Maximum velocity	V_{max}	5	mol m^{-3} s^{-1}
Hydrolysis rate constant	k_h	0.1	s^{-1}

All terms in the model are dimensionless. Parameters for starch kinetics are adapted from Sun & Henson (1990), Frandsen & Svensson (1998), Liesche *et al*. (2021).

intercellular interface and, thus, the strength of osmotic effects. This coefficient remains undefined between tracheary elements (ax, tt), since it is only relevant for connections involving living cells (σ_{pd}, σ_{aq}). When $\sigma_{ij} = 1$, the membrane is impermeable to the solute, so a gradient in the osmotic pressure can be fully established. When $\sigma_{ij} = 0$, the solute can freely pass through the interface, and its flow is directly coupled to the water flow. For connections between a living and a tracheary cell, which are mediated by aquaporins, $\sigma_{ij} = \sigma_{aq} = 1$. The reflection coefficient between two living cells, σ_{pd}, approaches 0 but can be varied within the model to bias the relative abundance and accessibility of aquaporins (higher σ_{ij}) vs plasmodesmata (lower σ_{ij}), since sugar can pass through plasmodesmata but not through aquaporins.

Sugar is only present in the living cells, where it can only flow symplasmically (via the cell lumen) (Gao *et al*., 2023). As a consequence, there is no sugar flow into or through the tracheary elements, whose sugar concentration is always zero. The model assumes that sugar is transported passively without the input of metabolic energy, as is generally believed in conifers. Though sugar transporters have been found in conifers, their function within the leaves remains unclear, and we ignore their potential contributions in our model (Han *et al*., 2022). The sugar flow J_{ij} is described by an advection–diffusion equation:

$$J_{ij} = \left(1 - \sigma_{ij}\right) U_{ij}\, \bar{c}_{ij} + \omega_{ij} RT \Delta c_{ij} \qquad \text{Eqn 2}$$

where $\bar{c}_{ij}$ is the mean concentration of nodes i and j, a valid approximation for a low Péclet number regime. The factor $\omega_{ij}RT$ serves as an effective diffusion coefficient, where the solute mobility ω_{ij} is a function of the size and abundance of plasmodesmata, along with the free diffusion of sugar, and depends on ξ_{ij} (Dechadilok & Deen, 2006; Bohr *et al*., 2018) (see Supporting Information).

Table 2 Summary of the relative intercellular conductivities, ξ_{ij}, for each cell pair.

		Tracheary		Living			
		ax ▲	tt ♦	ap ▼	tp ●	en ■	ms ♦
Tracheary	ax ▲	Bordered pits		Aquaporins			
	tt ♦	Water only		Water only			
		$\xi_{bp} = 1$		$0 \le \xi_{aq} < 1$			
Living	ap ▼	Aquaporins		Plasmodesmata and Aquaporins			
	tp ●	Water only		Sugar and water			
	en ■	$0 \le \xi_{aq} < 1$		$0 < \xi_{pd} < 1$			
	ms ♦						

ap, Axial phloem (magenta downward triangles); ax, axial xylem (dark blue triangles); en, endodermis (light green squares); ms, mesophyll (dark green diamonds); tp, transfusion parenchyma (orange circles); tt, transfusion tracheid (cyan diamonds).

Starch synthesis and hydrolysis are enzyme-mediated processes (Zeeman *et al.*, 2007). We approximate starch (s_i) dynamics using Michaelis–Menten enzyme kinetics:

$$\frac{ds_i}{dt} = M_s \frac{V_{max} c_i}{K_m + c_i} - k_h s_i \quad \text{Eqn 3}$$

where M_s is the molar mass of sucrose, V_{max} is the maximal velocity of starch synthesis, K_m is the Michaelis constant, and k_h is the rate constant for starch hydrolysis. The net change in sugar concentration in node i is a function of both transport and sequestration:

$$\frac{dc_i}{dt} = \sum_j J_{ij} - \frac{1}{M_s}\frac{ds_i}{dt} \quad \text{Eqn 4}$$

Model constraints and boundary conditions

For an incompressible fluid, mass conservation is ensured by continuity:

$$U_i = \sum_j U_{ij} + U_{i,bc} = 0 \quad \text{Eqn 5}$$

where $U_{i,bc}$ accounts for the water flows into node i from its relevant boundaries. For the transfusion tracheids and transfusion parenchyma, this term is zero. The axial xylem is connected to a distant water source at the roots with a fixed pressure (P_x, 0 MPa). The axial phloem is connected to a distant sugar sink with a fixed positive pressure (P_p, 0.1 MPa) and a sugar concentration of zero. The endodermal and mesophyll cells are subjected to a boundary condition representing the evaporative surfaces of the leaf near the stomata, where a net transpiration E is imposed. The per-area transpiration in pines has been estimated to be *c.* 1–5 mmol m^{-2} s^{-1} (Preisler *et al.*, 2023). In the model, E describes the net boundary flow from the endodermis and mesophyll, scaled by the molar volume of water, $\overline{v}$:

$$E = -\frac{1}{\overline{v}} \sum_{i \in en,\, ms} U_{i,bc} \quad \text{Eqn 6}$$

The mesophyll is assumed to be photosynthesizing at capacity, meaning its concentration never drops below c_m; however, in some instances, sugar is swept backward into a mesophyll cell. In this case, the concentration in the backwashed mesophyll cell is allowed to exceed c_m (Rockwell *et al.*, 2018). The model is allowed to evolve iteratively via Eqn 4 to a steady state, with the net sugar flux through each cell $J_i = \sum_j J_{ij} + J_{i,bc} = 0$ everywhere.

Results

Needle architecture and stelar tissue types

The cross-sectional distribution of tissues in the needle of *Pinus pinea* revealed, from outside to inside, the epidermis with stomata, mesophyll, and endodermis surrounding the stele with two vascular bundles embedded in the transfusion tissue. The architecture seen in both the fixed and stained material (fluorescence and electron micrographs; Fig. 2a,c) was well revealed in reconstructed cross sections from whole-needle, live μX-ray computed tomography. Here, the water-filled dead transfusion and xylem tracheids clearly contrast the living transfusion parenchyma, phloem, endodermal, and mesophyll cells (Fig. 2b). The transfusion tissue separated the endodermis and vascular bundles completely as seen in electron micrographs. It consisted of two cell types only, transfusion tracheids and transfusion parenchyma cells, the latter of which were characterized by dark tannin vacuoles and starch grains (Fig. 2c). Starch grains were also found in mesophyll and endodermal cells. The phloem flank was marked by a group of Strasburger cells, which aid with phloem loading, that otherwise occurred in phloem rays (Fig. 2c, yellow). The complexity of the interior of a conifer needle can be appreciated in 3D-visualizations based on the μX-ray tomography of the tip of a *P. pinea* leaf, where the tissues are identified by their tomography contrast and by tissue painting, respectively (Fig. 2d,e).

Model behavior

A representative steady-state solution of a network constructed from a *Pinus pinea* micrograph is shown in Fig. 3(b) (see Fig. S1 for an overlay with Fig. 2b). With the parameters listed in Table 1, the model reaches a steady state, and the direction of flow at the boundaries is consistent with biological expectations. Water exits the xylem and flows towards the sites of evaporation, and sugar moves from the sites of photosynthesis to the phloem loading point for export. Both pass through the endodermis between the transfusion tissue and the mesophyll. Upon exiting the endodermis, water continues to the airspaces, either directly or through the mesophyll, in agreement with current heat and mass transfer models of leaf vapor transport (Rockwell *et al.*, 2014a,b; Buckley *et al.*, 2017; Rockwell & Holbrook, 2017; Jain *et al.*, 2024a,b).

Redistribution of sugar is observed along the endodermis before entering the transfusion parenchyma. For an endodermal cell, the average ratio of its tangential sugar flow with neighboring endodermal cells to its radial sugar flow with transfusion parenchyma or mesophyll is 1.05 ± 0.20 (±SE). This indicates that the tangential flow along the endodermis is comparable to the radial flow across it, as the conductivity ξ_{pd} was chosen to be the same for all connections between living cells. This result is consistent with experimental observations of plasmodesmal density within the endodermis (Gao, 2022).

Quantitative analysis of cell-level physiological metrics within the stele is presented in Fig. 4. The water potential $\psi = P - RTc$ describes the chemical potential of water per molar volume, with water flowing from higher to lower water potentials. For tracheary elements, which do not have an osmotic component, this is equivalent to the pressure P. Away from the xylem, ψ becomes increasingly negative, driving water flow from the xylem to the rest of the needle, ending in the phloem to be exported as

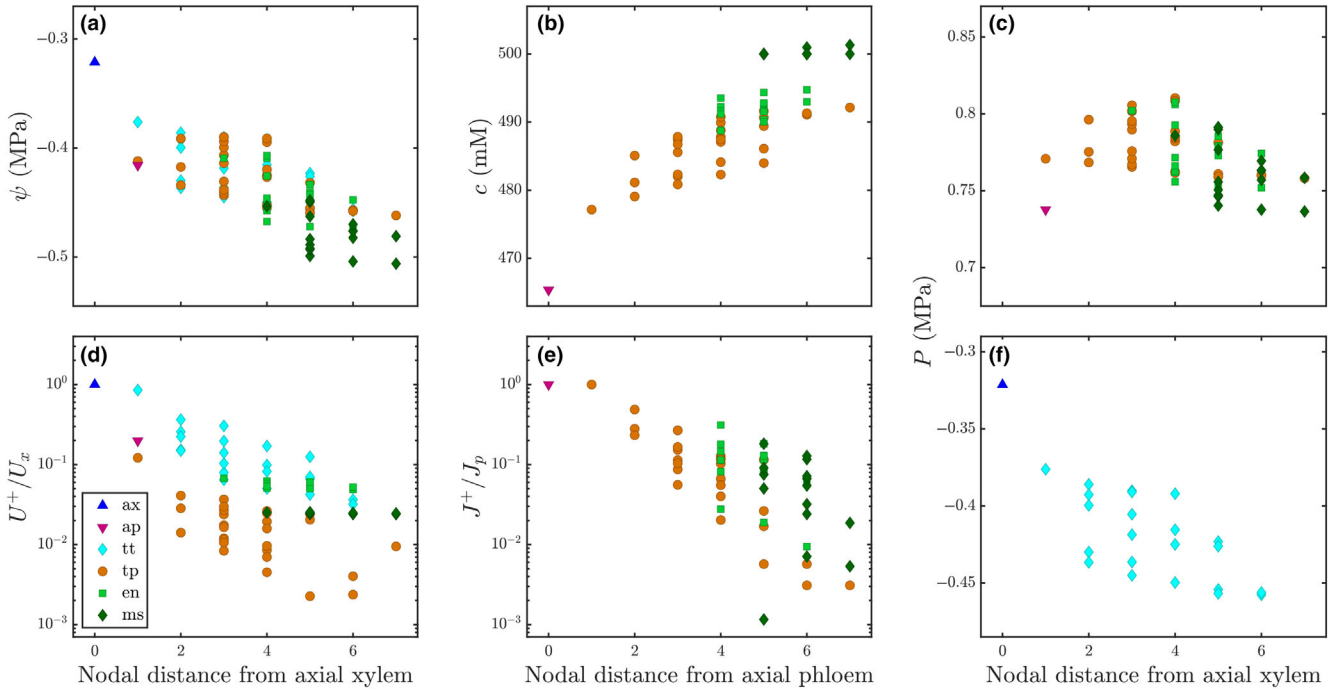

Fig. 4 The steady-state solution of a representative *Pinus pinea* network demonstrates the effect of cell position on flow. Sugar and water flows dissipate with nodal distance (shortest discrete path length) from the axial vasculature. Each point represents an individual cell (axial xylem (ax, dark blue triangles), axial phloem (ap, magenta downward triangles), transfusion tracheid (tt, cyan diamonds), transfusion parenchyma (tp, orange circles), endodermis (en, light green squares), and mesophyll (ms, dark green diamonds)). (a) Cell water potential ψ in relation to nodal distance from the axial xylem. (b) Sugar concentration c in the living cells in relation to nodal distance from the axial phloem. (c, f) Pressure P in living (c, positive pressure) and tracheary (f, negative pressure) cells with nodal distance from the axial xylem. The vertical axes for (c) and (f) share the same scale for comparison. (d, e) Relative flow rates through each cell are represented by the incoming water (U^+) and sugar (J^+) flows into each node, normalized by the total axial xylem water flux U_x or phloem sugar flux J_p, respectively.

sap, into the mesophyll for photosynthesis, or beyond the mesophyll to be evaporated near the stomata (Fig. 4a). The concentration profile (Fig. 4b) shows a downward gradient from the mesophyll to the phloem. Meanwhile, there is a minimal pressure gradient along that pathway through the living cells (Fig. 4c), especially compared to that of the tracheary system moving away from the xylem (Fig. 4f). This suggests sugar transport is a primarily diffusive, instead of advective, process through the plasmodesmata. This diffusive transport is consistent with the passive loading scheme in conifers.

At the interface between the endodermis and mesophyll, but elsewhere as well, sugar and water flows directly oppose each other. Fig. 4(d,e) show the incoming components of the total flow rates of water (U^+) and sugar (J^+) (such that $U_i^+ + U_i^- = U_i = 0$, or equivalently, $U_i^+ = \frac{1}{2}\sum_j \mid U_{ij} \mid$), normalized by the flows through the xylem (U_x) and phloem (J_p), respectively, for each node. Water fluxes through the transfusion parenchyma are approximately an order of magnitude slower than the fluxes through the tracheids, further supporting that sugar transport through the symplast is mostly diffusive instead of advective (Fig. 4d). The Péclet number is a dimensionless quantity that describes the ratio of advective and diffusive transport. At low Péclet numbers, only a small concentration gradient is required for the diffusive sugar current to overcome the advective water flow, allowing for bidirectional transport across an interface. By distributing flow from the focused vascular flank across multiple cells ultimately in the endodermis, the branching structure of the transfusion tissue slows down water flow by several orders of magnitude with increasing distance from the axial vasculature. Across the endodermis, the outward movement of water becomes slow enough to allow for low Péclet numbers. Sugar can diffuse inward against the water current, resolving the traffic jam of directly opposing flows at the endodermis.

Starch was added as a storage term for sugars. The inclusion of starch kinetics does not change the steady-state solution of pressures and sugar concentrations, regardless of the parameters chosen for Eqn 3, though the time to reach steady state and the final abundance of starch within the needle will be affected. No discernible variation in the spatial distribution of starch was observed in the model solution (Fig. S2).

Bundle size

To investigate the impact of an intermediary transfusion tissue on the constriction at the vascular access point, we examine a reduced version of the model. If the stele is fully occupied by the axial vasculature without any transfusion tissue, the needle can be represented by a ring of endodermal cells that are directly connected to the axial vasculature via a single cell at the flank (Fig. 5a(i)). We use the export efficiency J_p/E (μmol sugar per mol water) as a

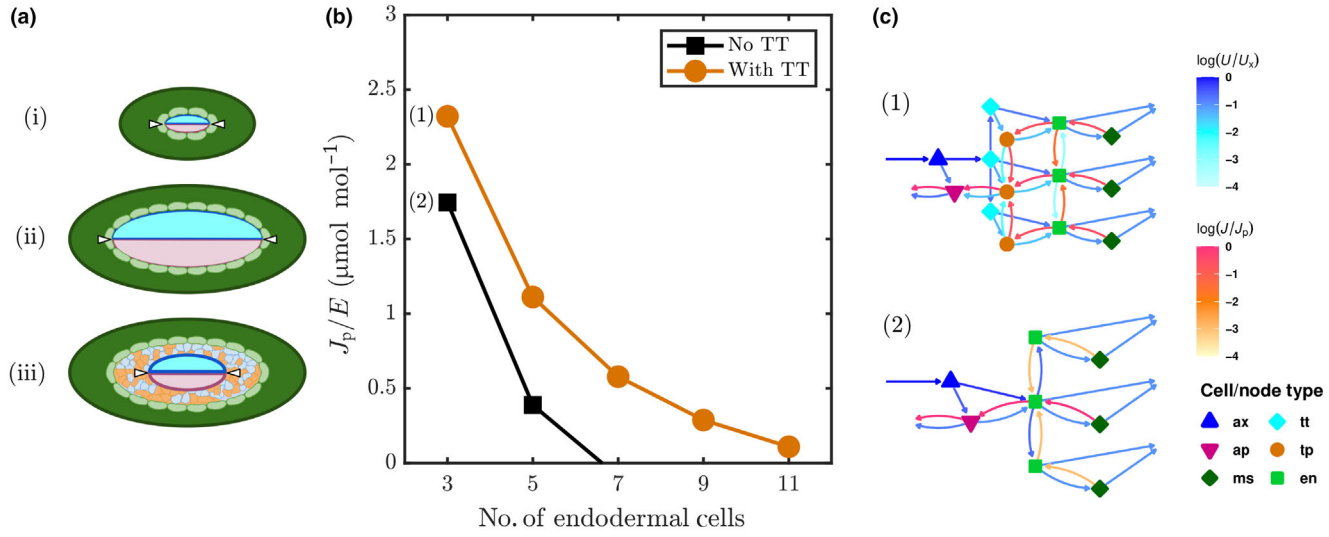

Fig. 5 The intervening transfusion tissue alleviates bottlenecking issues. (a) Cartoons of a hypothetical stele composed of only primary vascular tissue, xylem (blue) and phloem (magenta) (i). A larger stele is circumscribed by more endodermal cells (pale green) (ii). However, loading and unloading is still limited to the focal points (white arrows). Transfusion tissue can be inserted into the stele (iii). (b) Increasing the size of the stele with only axial vasculature results in a rapid loss of export efficiency, J_p/E (black squares). Including a single layer of transfusion tissue (orange circles) bolsters export for larger steles. Diagrams of the networks (1) and (2) are shown in (c), with arrows showing water (U, cyan to blue) and sugar (J, yellow to red) flows between cells, normalized to the flows through the axial xylem (U_x) and axial phloem (J_p), respectively. ax, axial xylem; ap, axial phloem; tt, transfusion tracheid; tp, transfusion parenchyma; en, endodermal cell; ms, mesophyll.

metric for assessing needle function. The export efficiency measures the amount of sugar loaded into the phloem relative to the amount of water lost to transpiration. At steady state, J_p is equivalent to the net assimilation. Increasing the radius of the stele can be represented by increasing the number of circumscribing endodermal cells (Fig. 5a(ii)). Regardless of bundle size, flows still must focus at the vascular flank, so increasing the size of the stele further exacerbates the existing bottleneck. This transformation towards a larger endodermal circumference diminishes the export efficiency J_p/E, until export becomes dysfunctional when the number of endodermal cells exceeds 5 (Fig. 5b, black squares).

For systems with multiple endodermal cells, which experience a constriction of flows at the vascular access points, inclusion of a single layer of transfusion tissue (Fig. 5c(1)) separates the water and sugar pathways interior to the endodermis, allowing bundles up to 11 cells to maintain a positive export efficiency (Fig. 5b, orange circles). We note that transport through a model with a single endodermal cell is one-dimensional, so adding in a single layer of transfusion tissue into this system marginally decreases the export efficiency by introducing extra resistance along the transport pathway. The networks constructed for the model, corresponding to the observed anatomy, averaged *c.* 15–20 endodermal cells. In these larger systems with more complicated connectivity profiles among cells, degeneracy in the possible pathways further distributes these flows to accommodate even larger steles (Fig. 5a(iii)).

Interfacial hydraulics

The analysis above has shown that the inclusion of transfusion tissue alleviates the constriction at the vascular flank, and now we explore how the structure of the transfusion tissue accomplishes this. *Pinus*-type transfusion tissue exhibits notable compositional and spatial heterogeneity in its partitioning between transfusion tracheids and transfusion parenchyma (Gao *et al.*, 2023). To investigate this, two regimes can be considered (Fig. 6a). We compare (i) a fully parenchymatous tissue with (ii) a heterogeneous case, similar to what is seen naturally. In the heterogeneous model (ii), the transfusion tracheid and parenchyma systems are both in contact with the endodermis but also highly interdigitated with each other, and aquaporins in the membranes of the transfusion parenchyma along their interface allow for water to flow between them. This water flow is dictated by the difference in the water potential, which includes hydrostatic and osmotic pressure terms. By shifting the model between this configuration and a fully parenchymatous one (i), we can test the importance of physically separating the net water and sugar currents on the export efficiency J_p/E.

This can be accomplished by altering *all* osmotic interfaces of the transfusion tracheids, which include the tracheid-to-parenchyma ($\xi_{tt:tp}$) and tracheid-to-endodermis ($\xi_{tt:en}$) conductivities. Fig. 6(b) shows the effect of this concurrent attenuation of both $\xi_{tt:tp}$ and $\xi_{tt:en}$, which together we define as the transfusion tracheids' aquaporin-mediated conductivity, $\xi_{tt:aq}$, on the export efficiency over all 66 constructed networks. It is important to note that only the conductivity of aquaporin-mediated interfaces of the transfusion tracheids are affected, while the conductivities between the axial xylem and either the axial phloem or adjacent transfusion parenchyma ($\xi_{ax:aq}$) remain constant. The landscape is further explored by sweeping over values for the plasmodesmata-mediated hydraulic conductivity among the living cells, ξ_{pd}, showing that export efficiency increases with

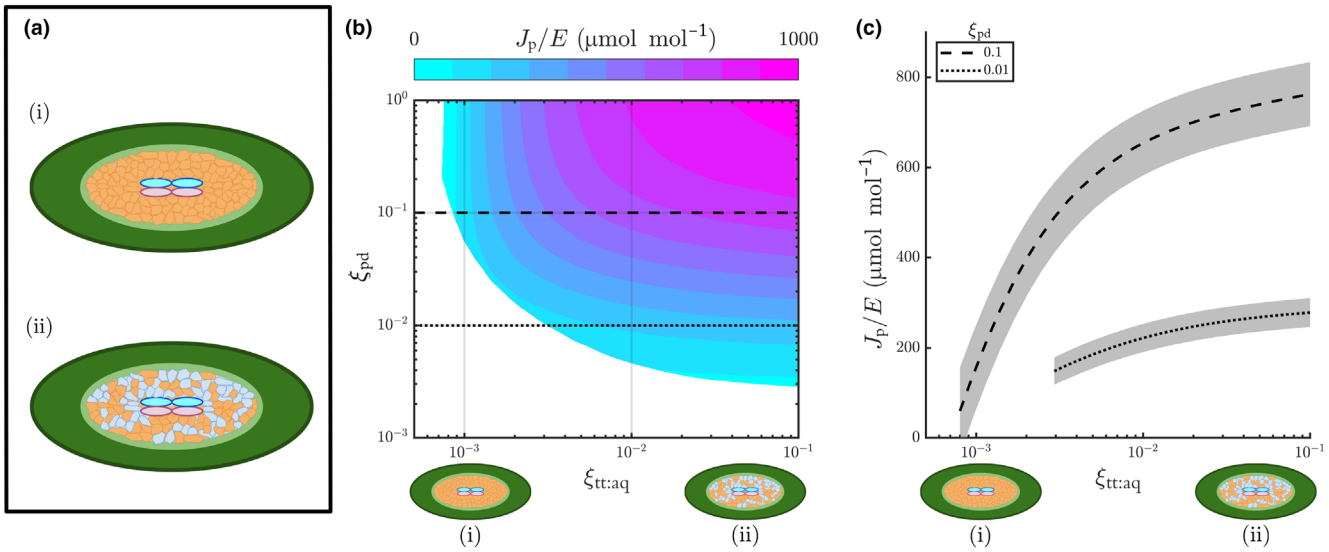

Fig. 6 The separation of water and sugar flows close to the vascular access points is crucial for needle function. (a) Conceptual schematics for hypothetical configurations of the stelar tissue. (i) A fully parenchymatous stelar tissue. (ii) A well-connected, heterogeneous transfusion tissue, with both the transfusion tracheid and transfusion parenchyma systems in contact with each other and with the endodermis. (b) Landscape of the export efficiency J_p/E (μmol sugar per mol water) between configurations (i) and (ii) by varying the aquaporin-mediated conductivity $\xi_{tt:aq}$ between transfusion tracheids and both the transfusion parenchyma and endodermis, relative to the plasmodesmata-mediated hydraulic conductivity between living cells ξ_{pd}. The landscape is averaged over 66 network configurations of *Pinus pinea* needles. Unshaded regions correspond to the parameter space which leads to negative sugar export and/or a loss of turgor. (c) Traces of the export efficiency landscape shown in (b) at $\xi_{pd} = 0.1$ (dashed) and 0.01 (dotted). Shading refers to the SD across all 66 configurations.

diminishing returns with increasing ξ_{pd}. Since $\xi_{tt:aq} \to 0$ severs the connections between transfusion tracheids and their neighboring transfusion parenchyma or the endodermis, the transfusion tracheid system becomes essentially nonfunctional or nonexistent at this limit (Fig. 6a(i)). Instead, water flows from the xylem directly into the transfusion parenchyma near the vascular flank and travels through the cell file into the endodermis, counter to the sugar current. Across the whole landscape, decreasing $\xi_{tt:aq}$ restricts export efficiency, leading to lower export relative to transpiration and eventually leading to total export dysfunction (Fig. 6b,c). As transfusion tracheids are removed from the system with decreasing $\xi_{tt:aq}$, water is forced to travel via the living tissue, frustrating the opposing flow of sugar and encountering greater resistance to irrigating the mesophyll. At this limit, the needle dries out and loses turgor.

We further probe the interfacial hydraulics of the transfusion tissue by examining the transfusion tracheid system's interactions with the transfusion parenchyma and endodermis separately. The large interfacial contact area between the transfusion tracheid and transfusion parenchyma systems suggests that hydraulic interactions between them may be important for function (Gao *et al.*, 2023). An internally disconnected system hydraulically separates the transfusion tracheids from the transfusion parenchyma but leaves the endodermis in direct contact with the transfusion tracheids. This could be conceived as a spatial separation and complete hydraulic disconnection of the two systems (Fig. S3A(ii)). For a more nuanced approach, this can be studied, as before, as an attenuation of aquaporin abundance at the transfusion tracheid:transfusion parenchyma interface by decreasing $\xi_{tt:tp}$ while keeping the tracheid:endodermis conductivity, $\xi_{tt:en}$, constant. Across a large range of ξ_{pd}, varying $\xi_{tt:tp}$ shows no appreciable effect (Fig. S3B), suggesting the interdigitation of the transfusion tracheid and parenchyma systems may be more of a developmental consequence than a critical feature for the internal irrigation of the transfusion tissue.

If, alternatively, the interdigitation is a mere morphological consequence allowing both the transfusion tracheids and the transfusion parenchyma to evenly service the entire endodermis, we instead study the importance of the direct irrigation of the endodermis via the transfusion tracheids (Fig. S3A(iii)). The hydraulic conductivity across this interface, $\xi_{tt:en}$ can be restricted while keeping $\xi_{tt:tp}$ unaffected. Even though water flow is limited directly between the transfusion tracheids and the endodermis, water can still enter the endodermis via the transfusion parenchyma. We do not study the case in which the transfusion parenchyma lose contact with the endodermis; since sugar can only flow through the transfusion parenchyma, severing its connection to the endodermis will obviously cause dysfunction. Altering these hydraulic connections between the transfusion tracheids and the endodermis also has no significant effect on export efficiency (Fig. S3C). This modification does little to change the behavior of the needle, since water can still enter the endodermis via adjacent transfusion parenchyma cells, which can draw water from the transfusion tracheids. In effect, this only extends the path length of the water flow by one cell.

Discussion

The transfusion tissue is a characteristic yet enigmatic feature of gymnosperm leaves and has been a subject of study since it was

first described by Frank (1864). Here we present a novel framework to understand the structural basis of its transport mechanics. Through a network model informed by anatomy, we argue that the transfusion tissue's heterogeneous composition and branching structure enable two-way transport of water and sugar between the mesophyll and the axial vasculature by dispersing the outward advective water flux and separating it from the inward diffusive sugar flux. By examining steady-state solutions of the model, we find that simultaneous transpiration and sugar export flows are possible. While starch dynamics likely improve export capacity by extending export after photosynthesis stops, our results indicate that these temporal processes are not strictly necessary for needle function.

The model provides cell-level resolution of water and sugar flows

We have developed a minimal mathematical model to resolve cell-level details of sugar and water flows through the transfusion tissue of conifer needles, a system that is difficult to probe experimentally. By exploring the parameter space, the model can overcome some deficiencies in empirical data to investigate how the structure of the transfusion tissue solves the architectural challenge of flow constriction at the focused vascular access points.

Moreover, the model is not limited to the *Pinus*-type transfusion tissue described by Hu & Yao (1981) and is widely applicable to diverse configurations of transfusion tissue. This versatility with respect to both configurations and boundary conditions underscores the model's utility in predicting needle function under several physiological conditions. While the presented analysis has been of steady-state solutions, the model can be adapted to understand temporal dynamics in response to environmental stimuli.

Flow through the endodermis

The Casparian strip at the endodermis forces water to move symplasmically across the endodermis via the plasmodesmata or aquaporins (Haberlandt, 1914; Wu *et al.*, 2005; Gao *et al.*, 2023). The branching of flows from the vasculature toward the endodermis allows the flow velocities to be quite low at the endodermis. At these small Péclet numbers, only small concentration gradients are necessary to generate a diffusive sugar flow that opposes a convective flow (Rockwell *et al.*, 2018). In the network model, flow can be biased such that it moves entirely through the plasmodesmata by setting the reflection coefficient σ to zero, and bidirectional transport is still possible. Therefore, at this interface of the endodermis, opposing flows of water and sugar may be established through not only the cell lumen but also the plasmodesmata. In real needles, water can also flow through aquaporins in the endodermis (Laur & Hacke, 2014). When the model accounts for the presence of aquaporins ($\sigma > 0$), this bidirectional flow becomes even easier to accomplish, as this opens another avenue for water to move separately from the sugar current.

Though the tiered architecture of the axial vasculature has been discovered, the exact local loading scheme into the phloem along the length of each tier remains unclear (Liesche *et al.*, 2021). Each segment is short enough for uniform loading along its length without stagnation, but it is also conceivable for sugars to be loaded primarily at the tip of each segment (Liesche *et al.*, 2021). External to the transfusion tissue, sugars can potentially travel axially down the endodermis and enter the stele in the plane at which a new set of vascular conduits appear. Yet, plasmodesmata-rich pit fields in the endodermis have been found in abundance in the tangential direction, in contrast with sparse plasmodesmata in the axial direction. This suggests that axial transport within the endodermis is limited compared to radial or tangential transport (Gao, 2022). Tangential redistribution of sugar along the endodermis before entering the transfusion tissue in the model is consistent with experimental observations of enrichment of plasmodesmata between endodermal cells. It is a reasonable assumption that tangential, but not axial, sugar flow in the endodermis indicates uniform axial loading of the phloem along a given segment. To interrogate this assumption, the current model may be extended to simulate concurrent axial and radial transport through networks built from three-dimensional reconstructions.

Partitioning of the transfusion tissue between tracheids and parenchyma

The transfusion tissue increases the size of the stele (Trueba *et al.*, 2022). A larger internal radius grants the annular mesophyll a larger photosynthetic surface area without increasing its thickness, which is limited by the depth of light penetration. Additionally, a larger bundle can improve needle irrigation (Rockwell & Holbrook, 2017). However, filling the stele entirely with axial vasculature exacerbates bottlenecking problems because loading is still limited to the vascular flanks. To overcome this problem while still increasing the size of the stele, including the intermediary transfusion tissue allows the flow to be distributed among many smaller pathways, eventually leading to low Péclet numbers at the endodermis, where the sugar and water flows directly oppose each other.

While building transfusion tissue to increase the size of the stele is favorable, the question becomes the partitioning of that space between transfusion tracheids and transfusion parenchyma. This can be simulated by reducing the hydraulic connection of the transfusion tracheids with both the transfusion parenchyma and the endodermis. Attenuating these conductivities forces water to travel through the parenchyma and decimates the ability of the needle to export sugar by forcing the direct opposition of the water and sugar currents and depressing the pressures within the living cells. On the other hand, increasing the internal irrigation of the transfusion tissue provides diminishing returns, similar to the vein density in angiosperms (Noblin *et al.*, 2008). Removing all transfusion parenchyma would lead to obvious dysfunction, since sugar can only travel symplasmically (Gao *et al.*, 2023). Between these two extremes, which both lead to failure, there must exist a partitioning of the transfusion tissue between transfusion tracheids and transfusion parenchyma that optimizes needle function. This likely depends on, among several factors, specific conductivity parameters and the relevant

optimization function and, while beyond the scope of the current study, is worthy of further research.

Extending the xylem via the transfusion tracheids towards the endodermis provides a low-resistance pathway for irrigation of the mesophyll. Moreover, extravascular irrigation is not limited to within the stele; in *Podocarpus*, 'accessory transfusion tracheids' extend the reach of the vasculature further into the mesophyll (Griffith, 1957; Brodribb & Feild, 2008). Yet, bringing the tracheids in contact with the endodermis does not seem to be the transfusion tissue's only advantage. Removing these direct connections effects little change, as long as the adjacent transfusion parenchyma cells are able to mediate the movement of water at that interface. By also severing the connection to the transfusion parenchyma, we find that the separation of flows within the transfusion tissue is critical for function. In the context of a bottlenecking problem, this becomes most important in regions close to the vascular focusing point, where velocities remain high. This issue is less severe further from this point, as flows slow down enough for diffusive currents to overcome advective ones. Rockwell & Holbrook (2017) report that, for angiosperms, which typically have much greater vein density, both the extravascular sugar and water currents have an effectively one-dimensional velocity profile. In other words, the flows move with a low, relatively constant velocity along their entire path, as opposed to focusing into or spreading out from a large advective velocity close to the vascular access points, as in gymnosperms. While a spatial separation of the two flows is not necessary for angiosperms, gymnosperms benefit from this strategy to manage the consequences of their vascular infrastructure.

Conclusion

While there has been significant work on the anatomy and development of the transfusion tissue, its physiology remains sparsely explored beyond its role in stress responses. Our results offer insights on the transfusion tissue's physiology under nonstressed conditions, suggesting that it separates and distributes fluid flow to overcome structural constrictions and support efficient irrigation and export.

The long, narrow geometry of conifer needles requires an architectural solution to efficiently traffic water and sugar along the leaf. To prevent axial stagnation, the axial vasculature develops tiers that segment the needle into separate, discrete loading zones. Consequently, only the outermost conduits of each segment are accessible for loading and unloading, forcing all radial water and sugar flows to focus from the entire needle circumference toward two points at the flanks. The transfusion tissue immediately separates the water and sugar pathways to reduce resistance between the vasculature and the endodermis. While the Casparian strip prevents the separation of water and sugar flows through the endodermis, the branched structure of the transfusion tissue dissipates flow velocities so that the advection of water and diffusion of sugar may directly oppose each other at that interface without frustrating sugar export.

Among several non-*Pinus* gymnosperms, there is still uncertainty whether a Casparian strip exists in the leaf endodermis. Where it is observed, there is likely variability in its permeability (Lersten, 1997; Liesche *et al.*, 2011). As such, directly opposing flows in the endodermal lumen (Fig. 1b) may not be a universal issue among gymnosperms. For example, in the U-shaped *Pseudotsuga*-type transfusion tissue, if the endodermal walls are partially permeable to water, apoplastic flow would relieve the endodermal bottleneck by reducing the need for the transfusion tissue to access all parts of the endodermis. To fully understand the context of different transfusion tissue morphologies, tracer studies can quantify the permeability of the endodermal apoplast (Gao *et al.*, 2023). However, constriction near the axial vasculature (Fig. 1a) is likely still relevant across gymnosperms. Even in the extinct genus *Cordaites*, accessibility of the vascular bundles appears similarly restricted to the flanks by strands of lignified sclerenchyma (Stopes, 1903; Costanza, 1985). We expect vascular constriction to still apply to extant gymnosperms. For instance, separating sugar and water flows would greatly reduce resistance between the opposing fluxes along the long, wing-like *Cupressus*-type transfusion tissue. Our model framework is flexible with respect to network configuration and can be utilized in concert with anatomical studies to interrogate the structure–function relationships of transfusion tissue more broadly across gymnosperms.

Acknowledgements

This work was supported by the Independent Research Fund Denmark in the grant Multimodal imaging and modelling of vascular flows in leaves (Grant no. 9040-00349B) and by the National Science Foundation through the Harvard University Materials Research Science and Engineering Center (DMR-2011754). We acknowledge the Paul Scherrer Institut, Villigen, Switzerland, for provision of synchrotron radiation beamtime at the TOMCAT beamline X02DA of the SLS and would like to thank Dr. Margaux Schmeltz for assistance. MHM recognizes support from the Fannie and John Hertz Foundation Fellowship and the National Science Foundation Graduate Research Fellowship (Grant no. DGE1745303) and thanks Sophie Everbach, Tinker Green, and Tony Rockwell for helpful discussions.

Competing interests

None declared.

Author contributions

MHM, NMH, AS and TB planned the research. CG and AS designed the imaging studies. CG, PARB and AS performed the imaging studies. MHM and TB designed the model. MHM performed the modeling studies. MHM, CG, PARB, NMH, AS and TB analyzed the data. MHM and AS wrote the paper with contributions from all authors.

ORCID

Tomas Bohr https://orcid.org/0000-0003-3620-7276
Peter A. R. Bork https://orcid.org/0000-0002-2577-6783

Chen Gao https://orcid.org/0000-0003-4750-3900
N. Michele Holbrook https://orcid.org/0000-0003-3325-5395
Melissa H. Mai https://orcid.org/0000-0002-9426-7018
Alexander Schulz https://orcid.org/0000-0001-6796-3598

Data availability

The codebase (developed with MATLAB2022b), along with a description of the algorithm and parameters, is available at https://github.com/melissahmai/transfusion_tissue.

References

Aloni R, Foster A, Mattsson J. 2013. Transfusion tracheids in the conifer leaves of *Thuja plicata* (Cupressaceae) are derived from parenchyma and their differentiation is induced by auxin. *American Journal of Botany* **100**: 1949–1956.

Bohr T, Rademaker H, Schulz A. 2018. Water motion and sugar translocation in leaves. In: Geitmann A, Gril J, eds. *Plant biomechanics: from structure to function at multiple scales*. Cham, Switzerland: Springer, 351–374.

Bouche PS, Delzon S, Choat B, Badel E, Brodribb TJ, Burlett R, Cochard H, Charra-Vaskou K, Lavigne B, Li S *et al.* 2016. Are needles of *Pinus pinaster* more vulnerable to xylem embolism than branches? New insights from X-ray computed tomography. *Plant, Cell & Environment* **39**: 860–870.

Brodribb TJ, Feild TS. 2008. Evolutionary significance of a flat-leaved *Pinus* in Vietnamese rainforest. *New Phytologist* **178**: 201–209.

Brodribb TJ, Holbrook NM. 2005. Water stress deforms tracheids peripheral to the leaf vein of a tropical conifer. *Plant Physiology* **137**: 1139–1146.

Buckley TN, John GP, Scoffoni C, Sack L. 2017. The sites of evaporation within leaves. *Plant Physiology* **173**: 1763–1782.

Canny MJ. 1993. Transfusion tissue of pine needles as a site of retrieval of solutes from the transpiration stream. *New Phytologist* **123**: 227–232.

Cardoso AA, Visel D, Kane CN, Batz TA, Sánchez CG, Kaack L, Lamarque LJ, Wagner Y, King A, Torres-Ruiz JM *et al.* 2020. Drought-induced lacuna formation in the stem causes hydraulic conductance to decline before xylem embolism in selaginella. *New Phytologist* **227**: 1804–1817.

Carter GM. 1911. A reconsideration of the origin of 'transfusion tissue'. *Annals of Botany* **25**: 975–982.

Carvalho MR, Turgeon R, Owens T, Niklas KJ. 2017. The hydraulic architecture of Ginkgo leaves. *American Journal of Botany* **104**: 1285–1298.

Chang CYY, Bräutigam K, Hüner NP, Ensminger I. 2021. Champions of winter survival: cold acclimation and molecular regulation of cold hardiness in evergreen conifers. *New Phytologist* **229**: 675–691.

Costanza SH. 1985. *Pennsylvanioxylon* of Middle and Upper Pennsylvanian coals from the Illinois Basin and its comparison with *Mesoxylon*. *Palaeontographica Abteilung B* **197**: 81–121.

Dechadilok P, Deen WM. 2006. Hindrance factors for diffusion and convection in pores. *Industrial and Engineering Chemistry Research* **45**: 6953–6959.

Esau K. 1977. *Anatomy of seed plants, 2nd edn.* New York, NY, USA: John Wiley and Sons.

Frandsen TP, Svensson B. 1998. Plant α-glucosidases of the glycoside hydrolase family 31. Molecular properties, substrate specificity, reaction mechanism, and comparison with family members of different origin. *Plant Molecular Biology* **37**: 1–13.

Frank AB. 1864. Ein Beitrag zur Kenntniss der Gefässbündel. *Botanische Zeitung* **22**: 149–156.

Furze ME, Trumbore S, Hartmann H. 2018. Detours on the phloem sugar highway: stem carbon storage and remobilization. *Current Opinion in Plant Biology* **43**: 89–95.

Gao C. 2022. *Multimodal imaging and functional anatomy of vascular flows in conifer needles*. PhD thesis, University of Copenhagen.

Gao C, Marker SJV, Gundlach C, Poulsen HF, Bohr T, Schulz A. 2023. Tracing the opposing assimilate and nutrient flows in live conifer needles. *Journal of Experimental Botany* **74**: 6677–6691.

Gersony JT, Hochberg U, Rockwell FE, Park M, Gauthier PP, Holbrook NM. 2020. Leaf carbon export and nonstructural carbohydrates in relation to diurnal water dynamics in mature oak trees. *Plant Physiology* **183**: 1612–1621.

Ghouse AKM, Khan MIH, Yunus M. 1972. The development of primary vascular elements in the needle leaves of *Pinus roxburghii*. *Bulletin of the Torrey Botanical Club* **99**: 190–195.

Ghouse AKM, Yunus M. 1974. Transfusion tissue in the leaves of *Cunninghamia lanceolata* (Lambert) Hooker (Taxodiaceae). *Botanical Journal of the Linnean Society* **69**: 147–151.

Ghouse AKM, Yunus M. 1975. Transfusion tissue in the leaves of *Thuja orientalis* L. *Annals of Botany* **39**: 225–227.

Gifford EM, Foster AS. 1996. *Morphology and evolution of vascular plants, 3rd edn.* New York, NY, USA: W. H. Freeman and Co.

Goldschmidt EE, Huber SC. 1992. Regulation of photosynthesis by end-product accumulation in leaves of plants storing starch, sucrose, and hexose sugars. *Plant Physiology* **99**: 1443–1448.

Goldstein RE, van de Meent JW. 2015. A physical perspective on cytoplasmic streaming. *Interface Focus* **5**: 20150030.

Griffith MM. 1957. Foliar ontogeny in *Podocarpus macrophyllus*, with special reference to transfusion tissue. *American Journal of Botany* **44**: 705–715.

Guzicka M, Marek S, Gawlak M, Tomaszewski D. 2023. Micromorphology of pine needle primordia and young needles after bud dormancy breaking. *Plants* **12**: 1–13.

Haberlandt G. 1914. *Physiological plant anatomy, 4th edn.* London, UK: Macmillian Co.

Han X, Gao C, Liang B, Cui J, Xu Q, Schulz A, Liesche J. 2022. 'Evidence for conifer sucrose transporters' functioning in the light-dependent adjustment of sugar allocation. *Tree Physiology* **42**: 488–500.

Heimerdinger G. 1951. Zur Mikrotopographie der Saftströme im Transfusionsgewebe der Koniferennadel II. Mitteilung. Entwicklungsgeschichte und Physiologie. *Planta* **40**: 93–111.

Hu Y-S, Yao B-J. 1981. Transfusion tissue in gymnosperm leaves. *Botanical Journal of the Linnean Society* **83**: 263–272.

Huber B. 1947. Zur Mikrotopographie der Saftströme im Transfusionsgewebe der Koniferennadel. I. Mitteilung. Anatomischer Teil. *Planta* **35**: 331–351.

Hunziker P, Schulz A. 2019. *Transmission electron microscopy of the phloem with minimal artifacts*. New York, NY, USA: Springer, 17–27.

Jain P, Huber AE, Rockwell FE, Sen S, Holbrook NM, Stroock AD. 2024a. Localized measurements of water potential reveal large loss of conductance in living tissues of maize leaves. *Plant Physiology* **194**: 2288–2300.

Jain P, Huber AE, Rockwell FE, Sen S, Holbrook NM, Stroock AD. 2024b. New approaches to dissect leaf hydraulics reveal large gradients in living tissues of tomato leaves. *New Phytologist* **242**: 453–465.

Jeffrey EC, Torrey RE. 1916. Ginkgo and the microsporangial mechanisms of the seed plants. *Botanical Gazette* **62**: 281–292.

Kedem O, Katchalsky A. 1958. Thermodynamic analysis of the permeability of biological membranes to non-electrolytes. *Biochimica et Biophysica Acta* **27**: 229–246.

Klages K, Donnison H, Wünsche J, Boldingh H. 2001. Diurnal changes in non-structural carbohydrates in leaves, phloem exudate and fruit in 'Braeburn' apple. *Australian Journal of Plant Physiology* **28**: 131–139.

Laur J, Hacke UG. 2014. Exploring *Picea glauca* aquaporins in the context of needle water uptake and xylem refilling. *New Phytologist* **203**: 388–400.

Lersten NR. 1997. Occurrence of endodermis with a Casparian strip in stem and leaf. *The Botanical Review* **63**: 265–272.

Liesche J. 2017. Sucrose transporters and plasmodesmal regulation in passive phloem loading. *Journal of Integrative Plant Biology* **59**: 311–321.

Liesche J, Martens HJ, Schulz A. 2011. Symplasmic transport and phloem loading in gymnosperm leaves. *Protoplasma* **248**: 181–190.

Liesche J, Schulz A. 2012. In vivo quantification of cell coupling in plants with different phloem-loading strategies. *Plant Physiology* **159**: 355–365.

Liesche J, Vincent C, Han X, Zwieniecki M, Schulz A, Gao C, Bravard R, Marker S, Bohr T. 2021. The mechanism of sugar export from long conifer needles. *New Phytologist* **230**: 1911–1924.

Noblin X, Mahadevan L, Coomaraswamy IA, Weitz DA, Holbrook NM, Zwieniecki MA. 2008. Optimal vein density in artificial and real leaves. *Proceedings of the National Academy of Sciences, USA* **105**: 9140–9144.

Preisler Y, Grünzweig JM, Ahiman O, Amer M, Oz I, Feng X, Muller JD, Ruehr N, Rotenberg E, Birami B *et al.* 2023. Vapour pressure deficit was not a primary limiting factor for gas exchange in an irrigated, mature dryland Aleppo pine forest. *Plant, Cell & Environment* **46**: 3775–3790.

Rademaker H, Jensen KH, Bohr T. 2021. Viscous energy dissipation in slender channels with porous or semipermeable walls. *Physical Review E* **103**: 1–5.

Rademaker H, Zwieniecki MA, Bohr T, Jensen KH. 2017. Sugar export limits size of conifer needles. *Physical Review E* **95**: 1–8.

Ribeiro RV, Machado EC, Habermann G, Santos MG, Oliveira RF. 2012. Seasonal effects on the relationship between photosynthesis and leaf carbohydrates in orange trees. *Functional Plant Biology* **39**: 471–480.

Rockwell FE, Gersony JT, Holbrook NM. 2018. Where does Münch flow begin? Sucrose transport in the pre-phloem path. *Current Opinion in Plant Biology* **43**: 101–107.

Rockwell FE, Holbrook NM. 2017. Leaf hydraulic architecture and stomatal conductance: a functional perspective. *Plant Physiology* **174**: 1996–2007.

Rockwell FE, Michele Holbrook N, Stroock AD. 2014a. Leaf hydraulics I: Scaling transport properties from single cells to tissues. *Journal of Theoretical Biology* **340**: 251–266.

Rockwell FE, Michele Holbrook N, Stroock AD. 2014b. Leaf hydraulics II: Vascularized tissues. *Journal of Theoretical Biology* **340**: 267–284.

Sands R, Correll RL. 1976. Water potential and leaf elongation in radiata pine and wheat. *Physiologia Plantarum* **37**: 293–297.

Stopes MC. 1903. On the leaf-structure of *Cordaites*. *New Phytologist* **2**(4/5): 91–98.

Sun Z, Henson CA. 1990. Degradation of native starch granules by barley α-glucosidases. *Plant Physiology* **94**: 320–327.

Tixier A, Orozco J, Roxas AA, Earles JM, Zwieniecki MA. 2018. Diurnal variation in nonstructural carbohydrate storage in trees: remobilization and vertical mixing. *Plant Physiology* **178**: 1602–1613.

Trueba S, Théroux-Rancourt G, Earles JM, Buckley TN, Love D, Johnson DM, Brodersen C. 2022. The three-dimensional construction of leaves is coordinated with water use efficiency in conifers. *New Phytologist* **233**: 851–861.

Webb W, Kilpatrick K. 1993. Starch content in Douglas-fir: diurnal and seasonal dynamics. *Forest Science* **39**: 359–367.

Worsdell WC. 1897. VIII. On "Transfusion-tissue": its origin and function in the leaves of gymnospermous plants. *Transactions of the Linnean Society of London. 2nd Series: Botany* **5**: 301–319.

Wu X, Lin J, Lin Q, Wang J, Schreiber L. 2005. Casparian strips in needles are more solute permeable than endodermal transport barriers in roots of *Pinus bungeana*. *Plant and Cell Physiology* **46**: 1799–1808.

Yang JY, Wei HB, Gou XD, Yang SL, Feng Z. 2022. Leaf anatomy of *Ningxiaites specialis* from the Lopingian of Northwest China. *Review of Palaeobotany and Palynology* **300**: 104632.

Zeeman SC, Smith SM, Smith AM. 2007. The diurnal metabolism of leaf starch. *Biochemical Journal* **401**: 13–28.

Zhang YJ, Hochberg U, Rockwell FE, Ponomarenko A, Chen YJ, Manandhar A, Graham AC, Holbrook NM. 2023. Xylem conduit deformation across vascular plants: an evolutionary spandrel or protective valve? *New Phytologist* **237**: 1242–1255.

Zhang YJ, Rockwell FE, Graham AC, Alexander T, Holbrook NM. 2016. Reversible leaf xylem collapse: a potential "circuit breaker" against cavitation. *Plant Physiology* **172**: 2261–2274.

Zhang YJ, Rockwell FE, Wheeler JK, Holbrook NM. 2014. Reversible deformation of transfusion tracheids in *Taxus baccata* is associated with a reversible decrease in leaf hydraulic conductance. *Plant Physiology* **165**: 1557–1565.

Zwieniecki MA, Stone HA, Leigh A, Boyce CK, Holbrook NM. 2006. Hydraulic design of pine needles: one-dimensional optimization for single-vein leaves. *Plant, Cell & Environment* **29**: 803–809.

Supporting Information

Additional Supporting Information may be found online in the Supporting Information section at the end of the article.

Fig. S1 Overlays of representative networks and their corresponding micrographs.

Fig. S2 Tangential distributions of starch content and pressure for the representative network.

Fig. S3 Parameter landscapes of export efficiency over isolated perturbations of the hydraulic conductivities between transfusion tracheids and transfusion parenchyma or the endodermis.

Notes S1 Nondimensionalization, relative conductivities, and effective diffusion.